Final Draft
of the original manuscript:

Huebner, P.; Zerbst, U.; Berger, M.; Brecht, T.:
The fracture of a wobbler in a heavy plate mill
In: Engineering Failure Analysis (2008) Elsevier

DOI: 10.1016/j.engfailanal.2008.06.021

THE FRACTURE OF A WOBBLER IN A HEAVY PLATE MILL

Peter Hübner [a], Uwe Zerbst [b], Maik Berger [c], Thomas Brecht [d]

[a] University of Applied Sciences, D-09648 Mittweida, Germany
[b] GKSS Research Centre, Institute of Materials Research, Materials Mechanics, D-21502 Geesthacht, Germany
[c] Technical University Chemnitz, D-09107 Chemnitz, Germany
[d] Ilsenburger Grobblech GmbH, 38871 Ilsenburg, Germany

Key words: heavy plate mill, wobbler, cleavage fracture, fracture mechanics, inspection regime

1. INTRODUCTION: BACKGROUND HISTORY AND AIM OF THE PRESENT INVESTIGATION

Wobblers are flexible couplings between the drive spindles and the working rolls of four-high rolling stands typically used for hot forming in heavy plate mills (**Figure 1**). Such a wobbler the diameter of which was about 1 meter failed by brittle fracture during a first pass this way causing the shutdown of the complete equipment. The subsequent failure investigation revealed the pre-existence of a fatigue crack of a depth of about a = 17 mm and a surface length of about 2c = 90 mm (**Figure 2**). Originating from this defect the cross section broke by a cleavage fracture mechanism. The result is schematically illustrated in **Figure 3**.

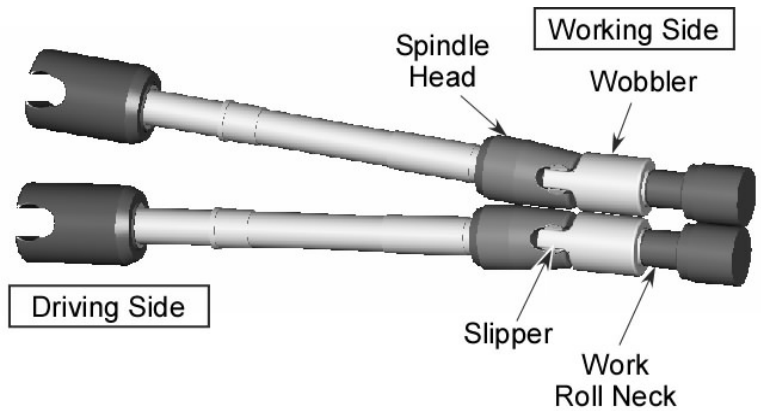

Figure 1: Schematic drawing of a wobbler connecting the driving shaft with the roll.

The aim of the present investigation was to simulate the failure from a fracture mechanics point of view. The underlying question was whether the damage was caused by inadequate design or by other reasons such as material defects, improper use in service or others.

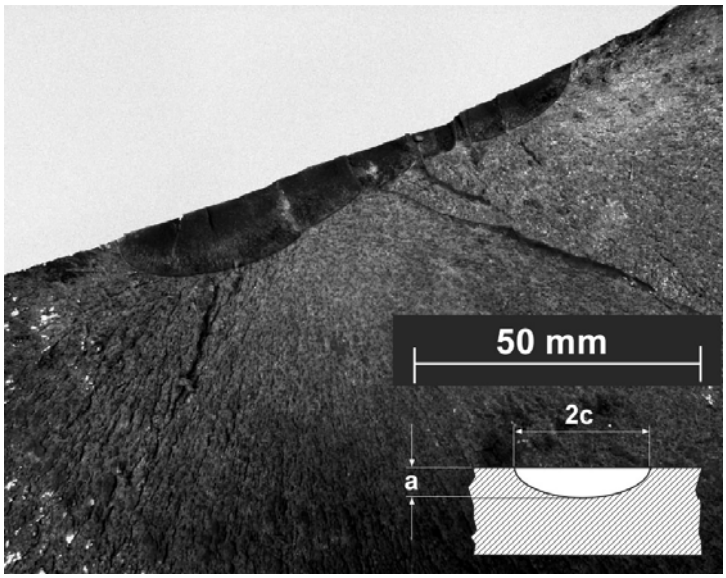

Figure 2: Fracture surface of the broken wobbler. The cleavage fracture event had its origin in a shallow fatigue crack at the surface.

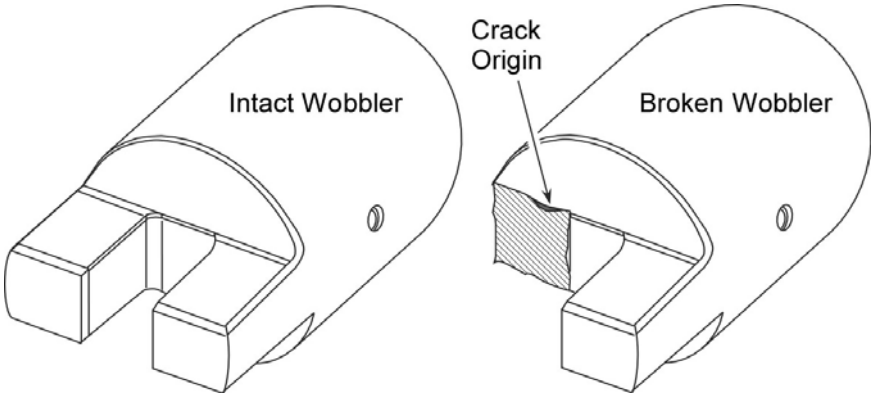

Figure 3: Schematic drawing of the broken wobbler.

For this purpose information had to be provided on

- The service loading of the component in terms of load spectra as well as the stress distribution across the relevant cross section as a function of the applied torsional moment,
- The initial crack size to be assumed as pre-existent in the analysis,
- The deformation behaviour of the material in terms of its stress-strain curve, and
- The crack propagation and fracture resistance of the material under static and cyclic loading.

Based on this information, the critical crack size and the residual lifetime subsequent to a routine inspection had to be determined by fracture mechanics analyses and compared with the real service conditions.

2. THE MATERIAL

The material was a quenched and tempered steel 34CrNiMo6 showing a yield strength of $R_{p0.2}$ = 807 MPa, an ultimate tensile strength of R_m = 948 MPa and an elongation at fracture of 14%. The temperature dependency of the Charpy energy is shown in **Figure 4**.

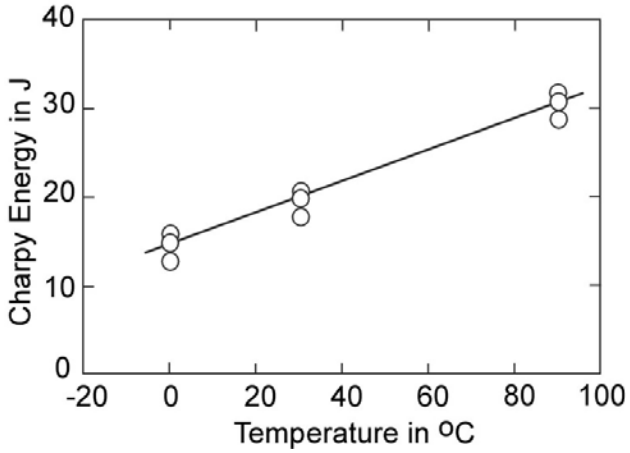

Figure 4: Temperature dependency of the Charpy energy of the steel investigated.

Fatigue crack propagation (da/dN-ΔK)-curves were determined for three R ratios (K_{min}/K_{max} = 0.1, 0.3 and 0.5) and processed to take into account crack closure effects. Basis for this was the so-called NASGRO approach [1]

$$\frac{da}{dN} = C \cdot \left[\left(\frac{1-f}{1-R} \right) \Delta K \right]^n \cdot \frac{\left(1-\Delta K_{th}/\Delta K\right)^p}{\left(1-K_{max}/K_c\right)^q} \tag{1}$$

which includes a specific crack closure function f

$$f = \frac{K_{op}}{K_{max}} = \begin{cases} \max\left(R,\ A_o + A_1 R + A_2 R^2 + A_3 R^3\right) & \text{for } 0 \le R \le 1 \\ A_o + A_1 R & \text{for } -2 \le R < 0 \end{cases} \tag{2}$$

with $$A_o = \left(0{,}825 - 0{,}34\alpha + 0{,}05\alpha^2\right) \cdot \left[\cos\left(\frac{\pi}{2} \cdot \frac{\sigma_{max}}{\sigma_o} \right) \right]^{1/\alpha}. \tag{3}$$

$$A_1 = \left(0{,}415 - 0{,}071\,\alpha\right) \cdot \frac{\sigma_{max}}{\sigma_o}, \tag{4}$$

$$A_2 = 1 - A_o - A_1 - A_3, \tag{5}$$

and $$A_3 = 2A_o + A_1 - 1. \tag{6}$$

In Eq.(3) σ_o is originally defined by the average between the static yield and tensile strengths and α is a constraint factor between 1 and 3. Following recommendations for steels in [1] the

authors have chosen $\sigma_{max}/\sigma_o = 0.3$ and $\alpha = 2.5$. The term $C\cdot\left[(1-f)/(1-R)\Delta K\right]^n$ in Eq. (1) represents the Paris equation modified for the stress ratio R, and the terms $(1-\Delta K_{th}/\Delta K)^p$ and $(1-K_{max}/K_c)^q$ model the S-shape of the curve; p and q are fit parameters chosen as p = q = 0.5. The Paris range of the da/dN-ΔK_{eff} curve ($\Delta K_{eff} = (1-f)/(1-R)\Delta K$) of the material is shown in **Figure 5** which also includes percentile values referring to probabilities of 5%, 20%, 50%, 80% and 95%. The statistical analysis is based on the C value of Eq. (1) and explained in detail in **Appendix A**. The fatigue crack propagation threshold ΔK_{th} was experimentally determined as $\Delta K_{th} = 6.0$ MPa·m$^{1/2}$ for an R ratio of R = 0. Note, however, that the subsequent analysis was carried out consistently taking into account crack closure. This includes the assumption that the only crack closure effect considered was the plasticity induced one.

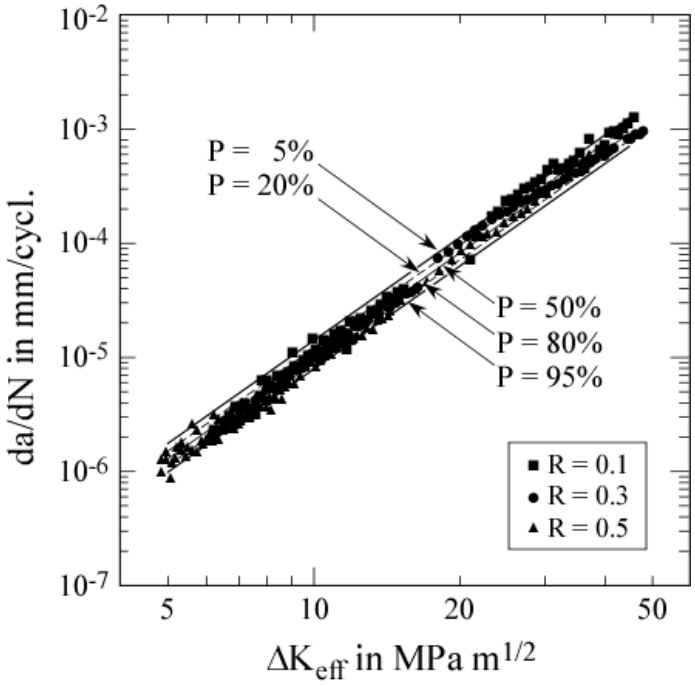

Figure 5: Paris range of the da/dN-ΔK_{eff} curve including percentile curves for various probabilities. These have been obtained as described in Appendix A.

The fracture mechanism is characterised by a ductile-to-brittle transition behaviour typical for ferritic and bainitic steels. A certain amount of stable ductile tearing is terminated by cleavage and the fracture resistance shows a considerable scatter band. Four toughness values have been determined and statistically processed by the Master Curve approach [2].[1)] Based on this the statistical distribution of **Figure 6** was obtained.

1) Note that this number of specimens does not really satisfy the requirements in [2] although the fracture resistance of all specimens was small enough to pass the census criterion.

Note that the toughness distribution is defined for so-called 1T specimens showing a crack front length of about 25 mm. The application to real structures, therefore, still requires a transformation with respect to the crack front length in the component under consideration. However, since the fracture resistance did not play an essential role in the subsequent residual lifetime analysis no details on this issue will be provided here.

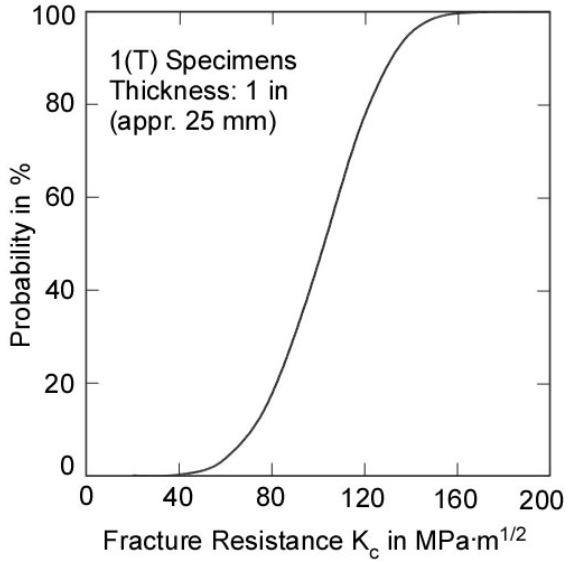

Figure 6: Fracture resistance distribution of the wobbler material at room temperature.

3. THE INITIAL CRACK SIZE

Initial cracks may have been introduced as incipient cracks during the manufacture of the components or they may have grown from defects and imperfections during service. In any case their existence has to be supposed in the analysis. What counts is the largest crack that could escape its detection by non-destructive inspection (NDI). This has to be chosen as the initial crack size the value of which, of cause, is largely dependent on the NDI method used in practice.

The wobbler of the present study was regularly investigated using a standard liquid penetrant technique and, additionally, at larger time intervals, by magnetic and ultrasonic techniques. For the present analysis a standard NDI initial crack size was chosen for the liquid penetrant method. This was a crack length at surface of $2c = 3.8$ mm (0.15 in.) for part through cracks of an aspect ratio $a/2c = 0.5$ in a heavy plate (thickness $t \geq 1.9$ mm/ 0.075 in.) [3].

4. THE LOADING CHARACTERISTICS

4.1 Stress Profile Across the Wall

Globally a wobbler is torsion loaded which is transferred as bending at the relevant cross section. Note that the loading pattern is not a trivial one since not the complete surface of the low ends is loaded but rather the edge regions. In order to cover this effect various loading

patterns have been simulated by finite element analyses. Finally the configuration shown in **Figure 7** was chosen as a slightly conservative alternative. The maximum principal stresses at surface due to a global torsional moment of 3000 kNm are shown in **Figure 8**.

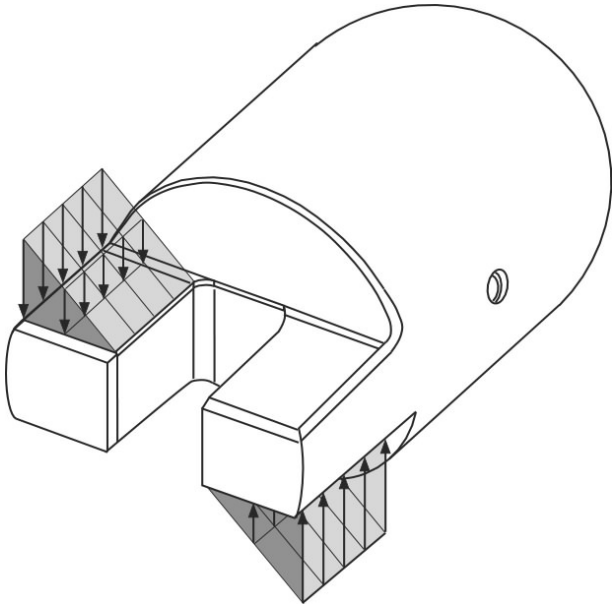

Figure 7: Loading of the low ends of the wobbler realised in the finite element analysis.

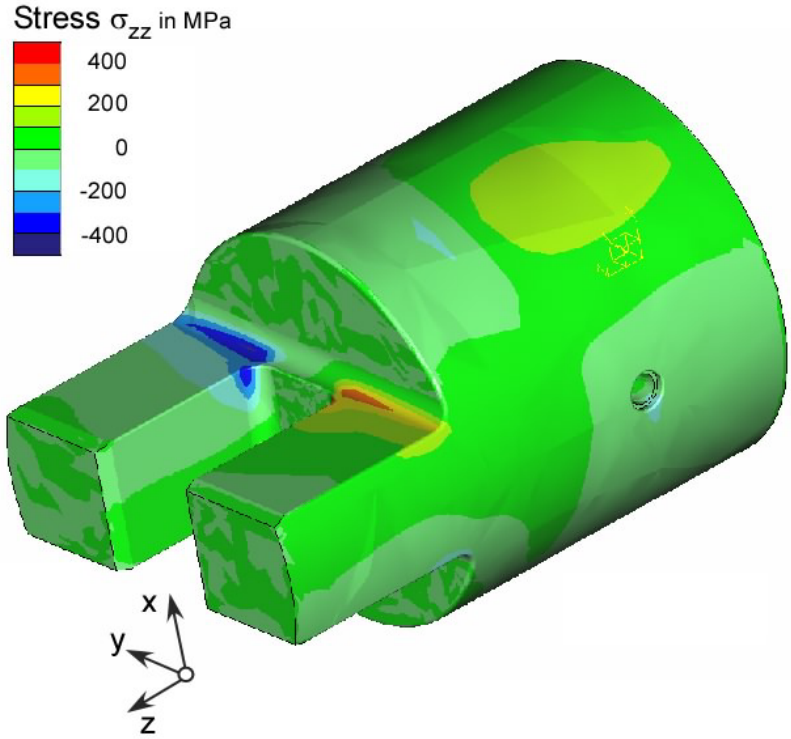

Figure 8: The maximum principal stresses at surface due to a global torsional moment of 3000 kNm.

4.2 Stress Intensity Factor

The stress intensity factors both for the deepest point (A) and the surface points (B) of the assumed crack were determined referring to a global torsional moment of 3000 kNm such as illustrated in **Figure 9**. For this the most critical through wall maximum principal stress profile from the finite element analysis was approximated by a polynomial

$$\sigma(x) = \sigma_0 + \sigma_1 \cdot x + \sigma_2 \cdot x^2 + \sigma_3 \cdot x^3 + \sigma_4 \cdot x^4 + \sigma_5 \cdot x^5 + \sigma_6 \cdot x^6 . \qquad (7)$$

The K factor was then determined by

$$K_I^A = \int_0^a \sigma(x) \cdot M_I^A(x,a)\,dx = \sigma_0 \cdot K_0^A + \sigma_1 \cdot K_1^A + \sigma_2 \cdot K_2^A + \sigma_3 \cdot K_3^A + \sigma_4 \cdot K_4^A + \sigma_5 \cdot K_5^A + \sigma_6 \cdot K_6^A \qquad (8)$$

for the deepest point of the crack (point A in Figure 9) and by

$$K_I^B = \int_0^a \sigma(x) \cdot M_I^B(x,a)\,dx = \sigma_0 \cdot K_0^B + \sigma_1 \cdot K_1^B + \sigma_2 \cdot K_2^B + \sigma_3 \cdot K_3^B + \sigma_4 \cdot K_4^B + \sigma_5 \cdot K_5^B + \sigma_6 \cdot K_6^B \qquad (9)$$

for the surface points of the crack (points B in Figure 9) [4]. The auxiliary functions K_i^A and K_i^B (i = 1…6) are given in **Appendix B**.

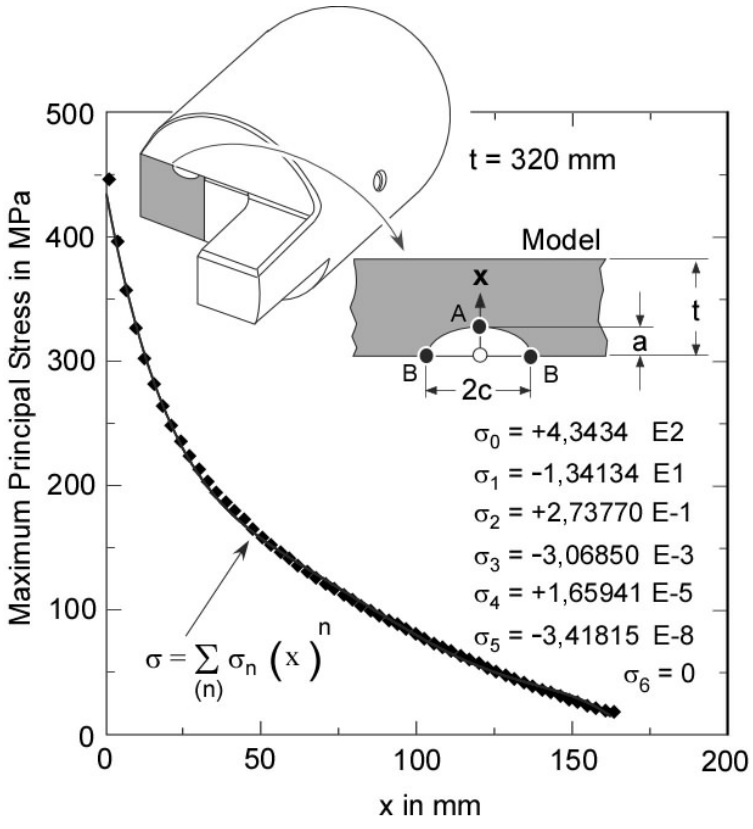

Figure 9: Approximation of the maximum finite element principal stress distribution across the relevant section by the polynomial of Eq. (7).

4.3 Loading Spectrum

As mentioned above the K factors of section 4.2 were determined for a global torsional moment of 3000 kNm. In reality the wobbler experienced a loading sequence comprising larger and smaller load amplitudes. It is common to re-arrange the loading data sequence as a loading spectrum displaying the loading amplitudes as a function of its occurrence. The present example spectrum for a time period of one year is shown in **Figure 10**. It is sorted such that it starts with the highest amplitude. In a fatigue crack propagation analysis the load spectrum is repeatedly applied to the structure until the critical crack size is reached. For this purpose the number of cycles of one spectrum can be varied proportionally. However, the highest amplitude must occur at least one times per spectrum. The K factors obtained by Eqs. (8) and (9) correlate proportionally to the referring bending stresses because of which they can simply be scaled in the fatigue crack propagation analysis.

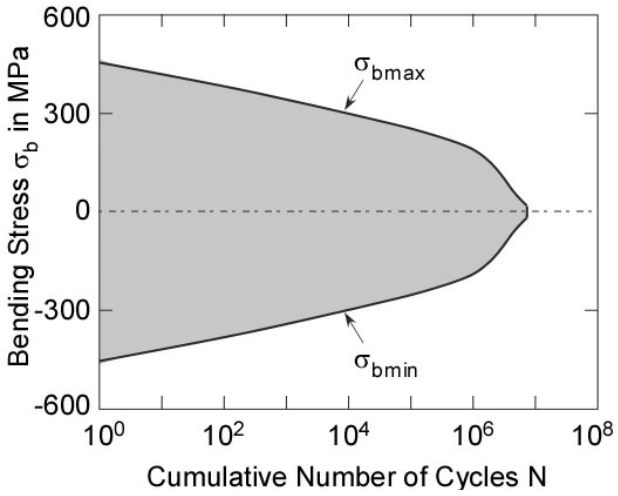

Figure 10: One year loading spectrum of the wobbler showing the maximum bending stress at the surface edge of the relevant section.

4.4 Ligament Yielding Parameter L_r

When the crack grows larger, ligament yielding effects have to be taken into account even at relatively low loads except for very brittle materials. The ligament yielding correction can be realised by multiplying the K factor by a term $1/f(L_r)$ which can easily be obtained by

$$f\left(L_r\right)=\left[\frac{E\cdot\varepsilon_{ref}}{\sigma_{ref}}+\frac{1}{2}\frac{L_r^2}{E\cdot\varepsilon_{ref}/\sigma_{ref}}\right]^{-1/2} \quad \text{for } 0\le L_r\le L_r^{max} \tag{10}$$

with σ_{ref} being a net section reference stress defined by

$$\sigma_{ref}=L_r\cdot\sigma_Y \quad . \tag{11}$$

and ε_{ref} being the according strain at the true stress-strain curve. For more detailed information see [5]. The parameter L_r is a measure of ligament yielding which, in the present example, was determined by

$$L_r = \frac{1}{(1-\zeta)^2 \sigma_Y} g(\zeta) \frac{\sigma_b}{3} + \sqrt{g^2(\zeta) \frac{\sigma_b^2}{9} + (1-\zeta)^2 \sigma_m^2} \,. \tag{12}$$

with $$g(\zeta) = 1 - 20\zeta^3 (a/2c)^{0.75} \quad . \tag{13}$$

and $$\varsigma = \frac{ac}{t(c+t)} \tag{14}$$

[6]. Eqs. (12) – (14) can be applied to plates large enough in comparison to the length of the crack so that edge effects do not influence the result, and to a crack depth no larger than 60% of the wall thickness if the loading is predominant bending [7]. L_r^{max} refers to the collapse limit of the structure simply determined by $L_r^{max} = 0.5 (\sigma_Y + R_m)$. The membrane and bending stresses, σ_m and σ_b, in Eq. (12) are given by

$$\sigma_m = \frac{1}{t} \int_0^t \sigma dx \tag{15}$$

and $$\sigma_b = \frac{6}{t^2} \int_0^t \sigma \left(\frac{t}{2} - x \right) dx \,. \tag{16}$$

If, as in the present case, the through thickness stress profile is available as a polynomial these equations can be solved as

$$\sigma_m = \sigma_0 + \frac{1}{2}\sigma_1 + \frac{1}{3}\sigma_2 + \frac{1}{4}\sigma_3 + \frac{1}{5}\sigma_4 + \frac{1}{6}\sigma_5 + \frac{1}{7}\sigma_6 \tag{17}$$

$$\sigma_b = -\frac{1}{2}\sigma_1 - \frac{1}{2}\sigma_2 - \frac{9}{20}\sigma_3 - \frac{2}{5}\sigma_4 - \frac{5}{14}\sigma_5 - \frac{9}{28}\sigma_6 \,. \tag{18}$$

If the polynomial is lower than sixth order the superflous σ_i coefficients are simply set to zero, e.q. for a polynomial of the third degree $\sigma_4 = \sigma_5 = \sigma_6 = 0$. Note that the specification of the σ_i coefficients is different to that of Eq. (7) such that it is referred to a relative distance (x/t) and not simply to x. The specification is given by

$$\sigma(x/t) = \sigma_0 + \sigma_1 (x/t) + \sigma_2 (x/t)^2 + \sigma_3 (x/t)^3 + \sigma_4 (x/t)^4 + ... \tag{19}$$

Note further that the definition of the membrane and bending stresses in Eqs. (15) and (16) is different to those commonly applied to K factor determination. For a more detailed discussion see again [5].

In **Figure 11** the finite element results, again for a global torsional moment of 3000 kNm, are plotted for both the tension and compression side of the plate. The offset in the centre of the plate is due to numerical effects. Nevertheless, the approximation by Eq. (18) is quite reasonably. Since the membrane stress σ_m = 0.2 MPa was much smaller than the bending stress σ_b = 297.4 MPa it was set to zero for the subsequent analysis.

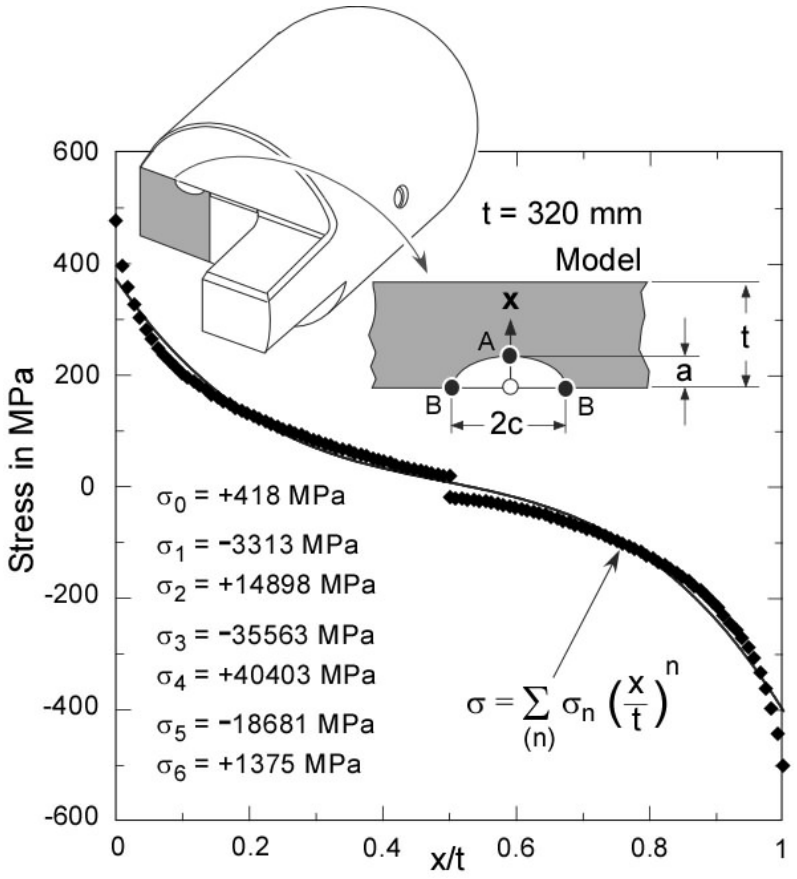

Figure 11: Approximation of the maximum finite element principal stress distribution across the relevant section by the polynomial of Eq. (19).

5. RESIDUAL LIFETIME ANALYSIS

The input information discussed so far was used for simulating the propagation of the initial fatigue crack of section 3. The analysis was performed consistently taking into account the crack closure effect, i.e., the crack driving force was determined in terms of ΔK_{eff} and the crack propagation was controlled by the da/dN-ΔK_{eff} curve and the threshold $\Delta K_{th,eff}$. The result of the analysis is shown in **Figure 12** for percentile values of 5 and 50% (cf. Figure 5). Whereas the 50% result gives the most probable scenario the 5% results defines an upper bound solution relevant for design purposes.

The crack depth versus loading cycles curves show a distinct pattern with retardation and acceleration phases of the crack propagation. The crack is accelerated at the beginning of the loading sequence with its high amplitude(s) and it decelerates at the end of the loading sequence which is characterised by small load amplitudes. Generally this “wiggles” could be smoothed out by proportionally shortening the individual loading sequences. However, as

already mentioned this is possible only as long as the highest load amplitude occurs at least one times per spectrum. Since exactly that was the case in Figure 12 no further smoothening was possible.

It was also mentioned that the exact measure of the fracture resistance did not play much a role in the analysis. As can be seen in Figure 6 the 5% probability value of the fracture resistance is as small as 67.3 $MPa\sqrt{m}$. This refers to a critical crack size in the order of a = 15 mm in Figure 12 (50% percentile curve) which is in good agreement with the crack size at real failure (Section 1). However, as can be seen from the curves in Figure 12 no much residual lifetime is left beyond this crack size. A crack depth of 15 mm refers to a number of loading cycles of approximately $12.6 \cdot 10^5$ (5% percentile value) and $22.5 \cdot 10^5$ (50% percentile value). If the wobbler were operated continuously this would refer to about 80 and 140 days respectively. However, in reality the same wobbler is not continuously operated for such a long time. Instead the tools are replaced about once per month and a routine inspection is carried out at this opportunity.

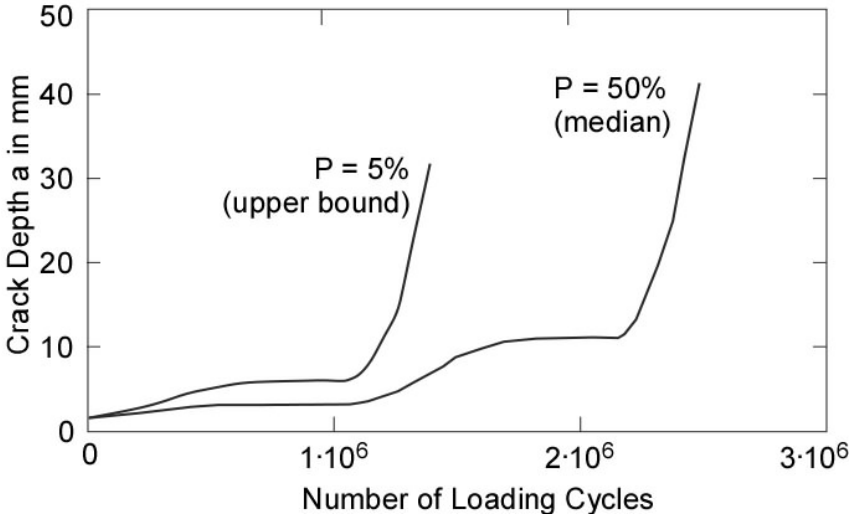

Figure 12: Results of the fatigue crack propagation and residual lifetime analysis. The percentile values of 5 and 50% refer to the curves in Figure 5.

6. CONCLUSIONS AND SUMMARY

The residual lifetime obtained in Figure 12 was shown to be too small for a meaningful inspection and maintenance regime which could accompany the service of the wobblers. Note that these wobblers were older tools and not originally developed for the new production line. In terms of the latter they were inadequately designed with the consequence of the failure event described above.

Since the performance could not be improved by accompanying measures the old wobblers were retired from service. At that time new equipment made of another material was already available. In addition the design was optimised with respect to the notch stresses.

Summarising, the example also shows that the fracture mechanics concept applied was a powerful tool for both explaining the failure event as well as improving the design of the structure.

6. LITERATURE

[1] NASGRO (2000): Fatigue Crack Growth Computer Program „NASGRO“, Version 3. NASA, L.B. Johnson Space Centre, Houston, Texas. JSC-22267B.

[2] ASTM E 1921-97 (1997): Standard test method for determination of reference temperature, T_o, for ferritic steels in the transition range. American Society for Testing and Materials.

[3] Farahamad, B., Bockrath, G. und Glassco, J. (1997): Fatigue and Fracture Mechanics of High Risk Parts. Chapman Hall, Int. Thomson Publ., Newe York et al., Section 5.3: Nondestuctive Inspection Techniques, pp. 269-288.

[4] Shen, G., Plumtree, A. and Glinka, G. (1991): Weight function for the surface point of semi-elliptical surface crack in a finite thickness plate. Engng. Fracture Mech. 40, pp. 167-176.

[5] Zerbst, U., Schödel, M., Webster, S. und Ainsworth, R.A. (2007): Fitness-for-Service Fracture Assessment of Structures Containing Cracks. A Workbook based on the European SINTAP/FITNET Procedure. Elsevier-Verl., Amsterdam, Bosten, Heidelberg, London, New York, Oxford, Paris, San Diego, San Francisco, Singapore, Sydney Sydney und Tokio.

[6] Sattari-Far, I. (1994): Finite element analysis of limit loads for surface cracks in plates. Int. J. Pressure Vessel Piping 57, pp. 237-243.

[7] R6, Revision 4: Assessment of the Integrity of Structures Containing Defects. British Energy Generation Ltd (BEGL), Barnwood, Gloucester 2004, Chapter IV.1: Limit load solutions for homogenous components.

Appendix A: Statistical processing of the Paris line of the da/dN-ΔK_{eff} curve

The percentile curves in Figure 5 were obtained by a stepwise procedure:

Step 1: All data points of the da/dN-ΔK_{eff} curve

$$\Delta K_{eff} = \left(\frac{1-f}{1-R}\right)\Delta K \tag{A1}$$

not belonging to the Paris range were eliminated by eye.

Step 2: The exponent n was fixed to n = 3 for steel. This allowed the determination of one C value for each of the remaining data points by

$$C = \frac{da/dN}{\Delta K_{eff}^{3}} \tag{A2}$$

Step 2: The resulting C values are sorted such that i = 1 referred to the smallest, i = N to the largest value. N was the overall number of data points, i was a counting parameter such that i = i to N.

Step 3: For each C value a probability P is determined by

$$P = i/N \tag{A3}$$

Step 4: This probability is plotted versus C such as shown in Figure A1. The percentile values for C then are simply taken from this curve.

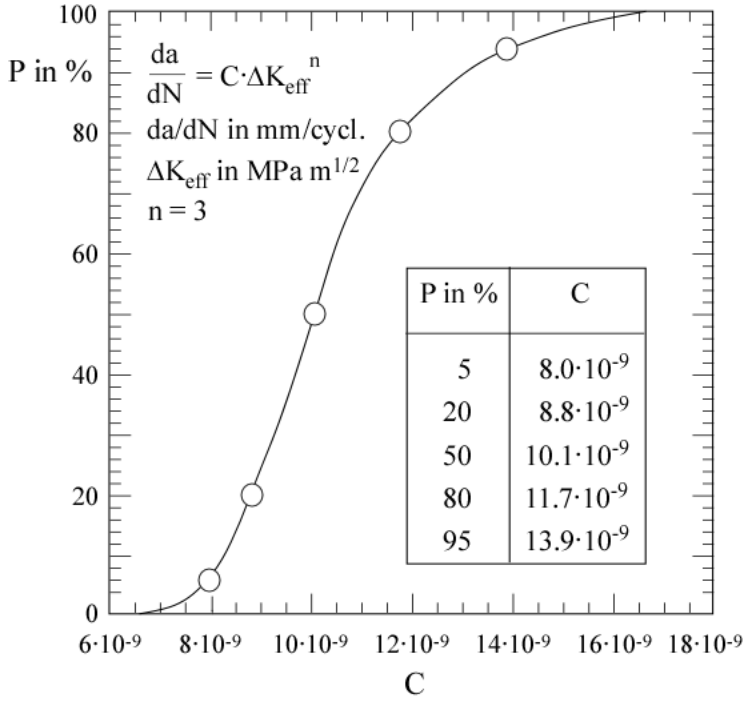

Figure A1: Empirical probability function of the C values referring to the Paris range of the da/dN-ΔK_{eff} curve of the present case study.

Appendix B: Auxilary functions referring to Eqs. (8) and (9) (according to [4]).

$$K_0^A = \int_0^a M_I^A(x,a)\,dx = \sqrt{\frac{2a}{\pi}} \cdot \left[2 + M_1^A + \frac{2}{3} M_2^A + \frac{1}{2} M_3^A \right] \tag{B1}$$

$$K_1^A = \int_0^a x \cdot M_I^A(x,a)\,dx = \sqrt{\frac{2a^3}{\pi}} \cdot \left[\frac{4}{3} + \frac{1}{2} M_1^A + \frac{4}{15} M_2^A + \frac{1}{6} M_3^A \right] \tag{B2}$$

$$K_2^A = \int_0^a x^2 \cdot M_I^A(x,a)\,dx = \sqrt{\frac{2a^5}{\pi}} \cdot \left[\frac{16}{15} + \frac{1}{3} M_1^A + \frac{16}{105} M_2^A + \frac{1}{12} M_3^A \right] \tag{B3}$$

$$K_3^A = \int_0^a x^3 \cdot M_I^A(x,a)\,dx = \sqrt{\frac{2a^7}{\pi}} \cdot \left[\frac{32}{35} + \frac{1}{4} M_1^A + \frac{32}{315} M_2^A + \frac{1}{20} M_3^A \right] \tag{B4}$$

$$K_4^A = \int_0^a x^4 \cdot M_I^A(x,a)\,dx = \sqrt{\frac{2a^9}{\pi}} \cdot \left[\frac{256}{315} + \frac{1}{5} M_1^A + \frac{256}{3465} M_2^A + \frac{1}{30} M_3^A \right] \tag{B5}$$

$$K_5^A = \int_0^a x^5 \cdot M_I^A(x,a)\,dx = \sqrt{\frac{2a^{11}}{\pi}} \cdot \left[\frac{512}{693} + \frac{1}{6} M_1^A + \frac{512}{9009} M_2^A + \frac{1}{42} M_3^A \right] \tag{B6}$$

$$K_6^A = \int_0^a x^6 \cdot M_I^A(x,a)\,dx = \sqrt{\frac{2a^{13}}{\pi}} \cdot \left[\frac{2048}{3003} + \frac{1}{7} M_1^A + \frac{2048}{45045} M_2^A + \frac{1}{56} M_3^A \right] \tag{B7}$$

$$K_0^B = \int_0^a M_I^B(x,a)\,dx = 2\sqrt{\frac{a}{\pi}} \cdot \left[2 + M_1^B + \frac{2}{3} M_2^B + \frac{1}{2} M_3^B \right] \tag{B8}$$

$$K_1^B = \int_0^a x \cdot M_I^B(x,a)\,dx = 2\sqrt{\frac{a^3}{\pi}} \cdot \left[\frac{2}{3} + \frac{1}{2} M_1^B + \frac{2}{5} M_2^B + \frac{1}{3} M_3^B \right] \tag{B9}$$

$$K_2^B = \int_0^a x^2 \cdot M_I^B(x,a)\,dx = 2\sqrt{\frac{a^5}{\pi}} \cdot \left[\frac{2}{5} + \frac{1}{3} M_1^B + \frac{2}{7} M_2^B + \frac{1}{4} M_3^B \right] \tag{B10}$$

$$K_3^B = \int_0^a x^3 \cdot M_I^B(x,a)\,dx = 2\sqrt{\frac{a^7}{\pi}} \cdot \left[\frac{2}{7} + \frac{1}{4} M_1^B + \frac{2}{9} M_2^B + \frac{1}{5} M_3^B \right] \tag{B11}$$

$$K_4^B = \int_0^a x^4 \cdot M_I^B(x,a)\,dx = 2\sqrt{\frac{a^9}{\pi}} \cdot \left[\frac{2}{9} + \frac{1}{5} M_1^B + \frac{2}{11} M_2^B + \frac{1}{6} M_3^B \right] \tag{B12}$$

$$K_5^B = \int_0^a x^5 \cdot M_I^B(x,a)\,dx = 2\sqrt{\frac{a^{11}}{\pi}} \cdot \left[\frac{2}{11} + \frac{1}{6} M_1^B + \frac{2}{13} M_2^B + \frac{1}{7} M_3^B \right] \tag{B13}$$

$$K_6^B = \int_0^a x^6 \cdot M_I^B(x,a)\,dx = 2\sqrt{\frac{a^{13}}{\pi}} \cdot \left[\frac{2}{13} + \frac{1}{7} M_1^B + \frac{2}{15} M_2^B + \frac{1}{8} M_3^B \right] \tag{B14}$$

$$M_I^A(x,a) = \frac{2}{\sqrt{2\pi(a-x)}} \left\{ 1 + M_1^A \cdot \left[1 - \frac{x}{a} \right]^{1/2} + M_2^A \cdot \left[1 - \frac{x}{a} \right] + M_3^A \cdot \left[1 - \frac{x}{a} \right]^{3/2} \right\} \tag{B15}$$

$$M_I^B(x,a) = \frac{2}{\sqrt{\pi \cdot x}}\left\{1 + M_1^B \cdot \left[\frac{x}{a}\right]^{1/2} + M_2^B \cdot \left[\frac{x}{a}\right] + M_3^B \cdot \left[\frac{x}{a}\right]^{3/2}\right\} \quad \text{(B16)}$$

$$M_1^A = \frac{\pi}{\sqrt{2Q}}\left[4Y_0 - 6Y_1\right] - \frac{24}{5} \quad \text{(B17)}$$

$$M_2^A = 3 \quad \text{(B18)}$$

$$M_3^A = 2 \cdot \left[\frac{\pi}{\sqrt{2Q}} \cdot Y_0 - M_1^A - 4\right] \quad \text{(B19)}$$

$$M_1^B = \frac{\pi}{\sqrt{4Q}}\left[30 \cdot F_2 - 18 \cdot F_1\right] - 8 \quad \text{(B20)}$$

$$M_2^B = \frac{\pi}{\sqrt{4Q}}\left[60 \cdot F_1 - 90 \cdot F_2\right] + 15 \quad \text{(B21)}$$

$$M_3^B = -\left[1 + M_1^B + M_2^B\right] \quad \text{(B22)}$$

$$Y_0 = B_0 + B_1 \cdot \left[\frac{a}{t}\right]^2 + B_2 \cdot \left[\frac{a}{t}\right]^4 \quad \text{(B23)}$$

$$B_0 = 1.10190 - 0.019863 \cdot \left[\frac{a}{c}\right] - 0.043588 \cdot \left[\frac{a}{c}\right]^2 \quad \text{(B24)}$$

$$B_1 = 4.32489 - 14.9372 \cdot \left[\frac{a}{c}\right] + 19.4389 \cdot \left[\frac{a}{c}\right]^2 - 8.52318 \cdot \left[\frac{a}{c}\right]^3 \quad \text{(B25)}$$

$$B_2 = -3.03329 + 9.96083 \cdot \left[\frac{a}{c}\right] - 12.582 \cdot \left[\frac{a}{c}\right]^2 + 5.3462 \cdot \left[\frac{a}{c}\right]^3 \quad \text{(B26)}$$

$$Y_1 = A_0 + A_1 \cdot \left[\frac{a}{t}\right]^2 + A_2 \cdot \left[\frac{a}{t}\right]^2 \quad \text{(B27)}$$

$$A_0 = 0.456128 - 0.114206 \cdot \left[\frac{a}{c}\right] - 0.046523 \cdot \left[\frac{a}{c}\right]^2 \quad \text{(B28)}$$

$$A_1 = 3.022 - 10.8679 \cdot \left[\frac{a}{c}\right] + 14.94 \cdot \left[\frac{a}{c}\right]^2 - 6.8537 \cdot \left[\frac{a}{c}\right]^3 \quad \text{(B29)}$$

$$A_2 = -2.28655 + 7.88771 \cdot \left[\frac{a}{c}\right] - 11.0675 \cdot \left[\frac{a}{c}\right]^2 + 5.16354 \cdot \left[\frac{a}{c}\right]^3 \quad \text{(B30)}$$

$$Q = 1 + 1.464 \cdot \left[\frac{a}{c}\right]^{1.65} \quad \text{for } \frac{a}{c} \le 1 \quad \text{(B31)}$$

$$F_1 = \alpha \cdot \left[\frac{a}{c}\right]^{\beta} \quad \text{(B32)}$$

$$F_2 = \gamma \cdot \left[\frac{a}{c}\right]^{\delta} \quad \text{(B33)}$$

$$\alpha = 1.14326 + 0.0175996 \cdot \left[\frac{a}{t}\right] + 0.501001 \cdot \left[\frac{a}{t}\right]^2 \quad \text{(B34)}$$

$$\beta = 0.458320 - 0.102985 \cdot \left[\frac{a}{t}\right] - 0.398175 \cdot \left[\frac{a}{t}\right]^2 \quad \text{(B35)}$$

$$\gamma = 0.976770 - 0.131975 \cdot \left[\frac{a}{t}\right] + 0.484875 \cdot \left[\frac{a}{t}\right]^2 \quad \text{(B36)}$$

$$\delta = 0.448863 - 0.173295 \cdot \left[\frac{a}{t}\right] - 0.267775 \cdot \left[\frac{a}{t}\right]^2 \quad \text{(B37)}$$

NOMENCLATURE

a	Crack depth (Figure 2)
c	Half crack length in surface direction (Figure 2)
C, n	Fitting parameters of the Paris range of the da/dN-ΔK curve
da/dN	Fatigue crack propagation rate
f	Crack closure function (Eq. 2)
K	Stress intensity factor (K factor)
K_c	Fracture resistance of the material
K_{max}	Upper K factor (cyclic loading)
K_{min}	Lower K factor (cyclic loading)
K_{op}	K factor referring to crack opening (cyclic loading)
L_r	Ligament yielding parameter (= σ_{ref}/σ_Y)
L_r^{max}	Plastic collapse limit L_r value
N	Cumulative number of loading cycles
N	Number of da/dN-ΔK_{eff} data points (Appendix A)
P	Probability
R	Stress ratio in fatigue crack propagation, R = K_{min}/K_{max}
t	Wall thickness of the component

α	Constraint parameter (Eqs. 3 and 4)
ΔK	Stress intensity factor range, $\Delta K = K_{max} - K_{min}$
ΔK_{eff}	Crack closure corrected effective ΔK
ΔK_{th}	Threshold value of ΔK below which there is no crack propagation
ε_{ref}	Reference strain (referring to σ_{ref} in the true stress-strain curve)
σ	Stress
σ_o	Reference stress in Eqs. (3) and (4); usually chosen as $0.5\ (\sigma_Y + R_m)$
σ_b	Bending stress component
σ_m	Membrane stress component
σ_{ref}	Net section reference stress ($= L_r \cdot \sigma_Y$)
σ_Y	Yield strength (for materials with Lüders' plateau $\sigma_Y = R_{p0.2}$)

Indices

A	Deepest point of the crack (Figures 9 and 11)
B	Surface points of the crack (Figures 9 and 11)